Available online at www.sciencedirect.com

ScienceDirect

Energy Procedia 92 (2016) 434 – 442

Energy Procedia

6th International Conference on Silicon Photovoltaics, SiliconPV 2016

Simulation of 20.96% efficiency n-type Czochralski UMG silicon solar cell

Peiting Zheng[a], Fiacre.E.Rougieux[a], Chris Samundsett[a], Xinbo Yang[a], Yimao Wan[a], Julien Degoulange[b], Roland Einhaus[b], Pascal Rivat[c] and Daniel Macdonald[a]

[a]*Research School of Engineering, College of Engineering and Computer Science, The Australian National University, Canberra, ACT 2601, Australia*

[b]*Apollon Solar, 66 Cours Charlemegne, 69002, Lyon France*

[c]*FerroPem, 517 Avenue de la Boisse, 73025 Chambery Cedex, France*

Abstract

In this paper, we present the 3D simulation of>20% efficiency solar cells using *n*-type 100% Upgraded-Metallurgical Grade (UMG) Czochralski (CZ) silicon and Electronic Grade (EG) Float Zone (FZ) fabricated using the same process. The cells have a passivated emitter rear locally diffused (PERL) structure, with an etch-back approach on the rear to maintain high bulk lifetime in the cells via phosphorus gettering. Simulation ofthe power losses of both devices are analysed as a function of measured material and cell parameters, including minority carrier lifetime, reflectance, contact resistivity and recombination parameters of the diffused and non-diffused surfaces.

Peer review by the scientific conference committee of SiliconPV 2016 under responsibility of PSE AG.

*Keywords:*silicon; upgraded metallurgical grade; compensation; solar cell; modelling and simulation

1. Introduction

Upgraded Metallurgical-Grade (UMG) silicon has raised interest as a low cost alternative material for high efficiency silicon solar cells[1-5].Currently, the most widely used process to produce silicon for electronic and solar applications is the Siemens process, which is both energy intensive (purified through the gas phase) and requires heavy initial investments. UMG silicon feedstock is purified using a solid or liquid phase purification process, which can avoid high thermal budgets (lower energy consumption) and requires less expensive infrastructure. There have been a number of techniques developed to date to further purify Metallurgical-Grade silicon (MG-Si) through

Peer review by the scientific conference committee of SiliconPV 2016 under responsibility of PSE AG.
doi:10.1016/j.egypro.2016.07.124

metallurgical routes. The most commonly used methods are: directional solidification, acid leaching, slag treatments, plasma purification and evaporation under vacuum [6-13]. However, the efficiency of these methods is not as good as in the gas phase purification.Therefore, UMG silicon contains more impurities, especially shallow acceptors and donors (B, Al and P), which have relatively larger segregation coefficients[14, 15],and so are more difficult to remove, and the minority carrier lifetime is usually lower in the as-grown state. In addition, the remaining dopant atoms in the feedstock lead to material compensation, the carrier mobility is thus reduced, and the presence of boron leads to the formation of the boron-oxygen (BO) defect, even in *n*-type compensated UMG silicon wafers[16-18]. Recent improvements in the UMG purification process have led to an improvement in feedstock quality[19]. The efficiency of UMG silicon based solar cells has also improved dramatically. A 19.8% efficiency solar cell has been reported by Rougieux*et al.*[20] in 2015, followed by a 20.96% efficiency UMG silicon solar cell in 2016 [21].In this paper, we present 3D simulation results using Quokka[22] (a 3D semiconductor simulation tool), forthisrecent high efficiency (20.96%) silicon cell based on 100% solar-grade feedstock, using *n*-type Czochralski-grown wafers, and a 21.91% cell based on Electronic Grade (EG)FZ material using the same fabrication process.

2. Experimental methods

The cells simulatedwere from two different types of *n*-type monocrystalline silicon wafers. The first type was grown with 100% UMG silicon feedstock without adding electronic grade polysilicon feedstock using the Czochralski process. The second type was from a Float-Zone (FZ) grown ingot using standard electronic grade (EG) silicon feedstock. The UMG feedstock was produced by FerroPem in the framework of the PHOTOSIL project. The wafers had resistivities of 4 Ω.cm (solidified fraction *f*s=20%) for the UMG material and 1 Ω.cm for the EG wafers. The doping density of both phosphorus and boron was measured by Secondary Ion Mass Spectrometry (SIMS) analysis, showing that the UMG wafers had a boron concentration [B] = 1.27×10^{16}cm^{-3} and phosphorus concentration of [P] = 1.42×10^{16} cm^{-3}, which results in a net doping of $n_0 = 1.4\times10^{15}$cm^{-3}.

The cell structure used in this study is a Passivated Emitter Rear Locally-diffused (PERL) solar cell structure[23], specially adapted to maintain a high carrier lifetime in the UMG material, and is represented in Figure 1. The cells were 2 × 2 cm^2 in size. A key feature of the cell is a full area phosphorus diffusion on the rear side which is etched back to leave islands of n+ silicon under the rear side contacts. This allows effective phosphorus gettering of the wafer, while also permitting reduced recombination at the rear side. A more detailed description of the cell fabrication process can be found in [21]. The dimensions of the contacts and the properties of the cells, for example, sheet resistance of the diffusion are summarized in Table 2.

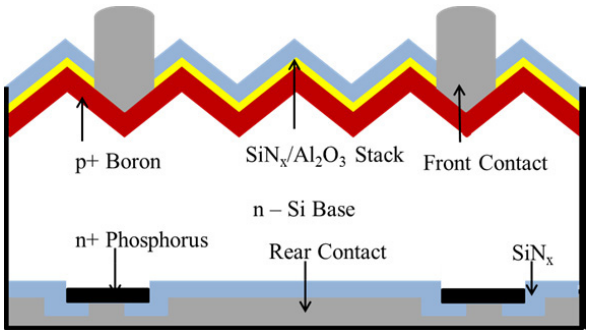

Fig. 1. Schematic diagram of PERL silicon solar cell with full front boron diffusion and rear etch-back localized phosphorus diffusion, Al_2O_3/SiN_xstack at the front and SiN_x at the rear side and with Cr/Pd/Ag stacks for both the front and rear contacts.The rear-side etch-back process results in the localized n+ phosphorus diffused regions.

In order to control the fabrication process and obtain accurate simulation results for the cells, several important parameters on control samples were measured. The recombination parameter J_0 of the front textured boron diffusion was measured on 100Ω.cm *n*-type control wafer. To measure the J_0 for the un-diffused rear side passivated with

SiN_x we used sister wafers to those used for cells.Dark IV measurements were performed using a Keithley 2400 source meter to extract the shunt resistance (R_{sh})[24]. The contact resistivity (ρ_c) for both the front and rear metallization was measured using Transfer Length Method (TLM) measurements[25]. Suns-V_{oc} measurements [26] were performed to evaluate the lumped series resistance (R_s) at maximum power point[27].

3. UMG material bulk lifetime study

Bulk lifetime is an important parameter to be used in the device simulation. It can significantly affect the recombination in the device, and thus the electrical properties of the cells. During the fabrication process, high temperature steps, for example, boron and phosphorus diffusion, can have a great impact on the bulk minority carrier lifetime. The accurate determination of the final bulk lifetime in the device is therefore critical for the accuracy of our simulations. The investigation of the bulk lifetime before and after each high temperature processes in this cell design has been reported in the previous study [21]. It showed that boron diffusion can dramatically reduce the carrier lifetime,by an order of magnitude. However, a subsequentphosphorus diffusion has a positivegettering effect and hence recovers the lifetime to some extent. Therefore an etch-back approach was utilized to achieve the localization of the diffusion on the rear side for the PERL structure to maintain a high bulk lifetime. A more detailed analysis on the bulk lifetime on both the UMG CZ and EG FZ wafers can be found in [21]. In this paper, only the final bulk lifetime after all high temperature processes for both UMG CZ and EG FZ wafers are shown. The injection dependent minority carrier lifetimes are used in the simulations in section 5.2. The final bulk lifetime for both types of wafers shown in Figure 2were measured down to an injection level of 10^{13} cm^{-3} for more accurate estimation of the bulk properties at low injection in the simulations. It is seen that the UMG CZ wafer has comparable bulk lifetime to the EG FZ wafer after high temperature processing, and has a slightly stronger injection dependence.

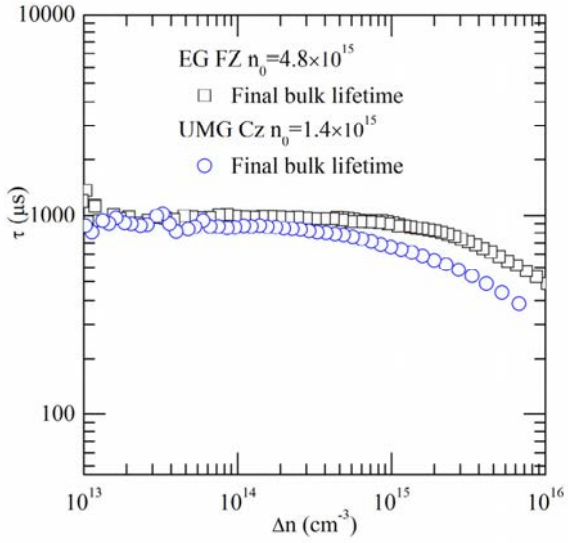

Fig. 2. Injection dependent minority carrier bulk lifetime for *n*-type EG 1 Ω.cm control wafer and*n*-type UMG Cz4 Ω.cm silicon wafers in the final state after all high temperature processes.

4. Cell results

Independent measurements of the illuminated current-voltage characteristics at FraunhoferCalLab confirm an efficiency of 20.96% and 21.91% for the best *n*-type UMG Cz cell and the best EG FZ cell. The IV curves together with the simulated light IV (to be discussed further in section 5) are plotted in Figure 3 (a). The thickness, dopant

concentrations, and net doping n_0 (n_0 = [P] – [B] for UMG material) of the cells are shown in Table 1. R_{sh}, $R_s$and pseudo fill factor (PFF) extracted from Dark-IV and Suns-V_{oc} measurements are also included in Table 1. The details of the extracted cell parameters from the illuminated IV curves are listed in Table 4.

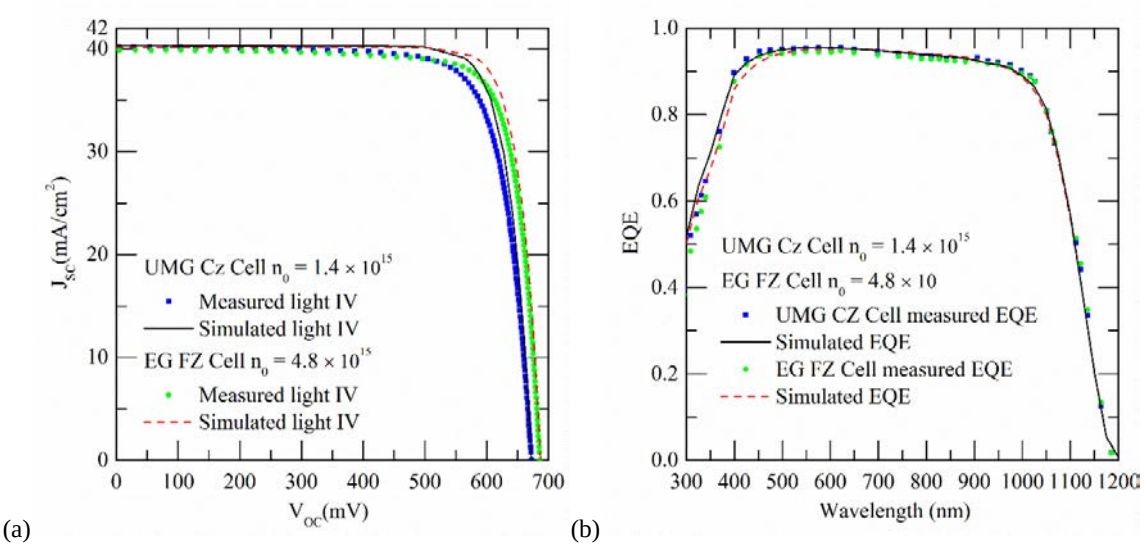

(a) (b)

Fig. 3. (a) Independent illuminated IV measurements at FraunhoferCalLab and simulated IV of the best *n*-type UMG Cz and EG FZ cells. (b) EQEmeasurements and simulation of the best *n*-type UMG Cz and EG FZ cells (measured at FraunhoferCalLab).

The External Quantum Efficiency (EQE) and the simulated EQE for the best cells are shown in Figure 3 (b).These reveal a slightly higher EQE for the UMG cell in the wavelength range from 300 to 900nm, especially in the range from 300nm to 600nm. This difference results from a slight difference in the thickness of the SiN_x capping layer on the front surface. This will be discussed in section 5.1 when simulating the reflectance of the cells.

Table 1. Dopant concentration and type, net doping n_0, thickness *W*and extracted cell parameters from illuminated IV curves of the UMG Cz and EG FZ cells

Parameters	UMG CZ	EG FZ
[P] (cm^{-3})	1.42×10^{16}	4.8×10^{15}
[B] (cm^{-3})	1.27×10^{16}	-
n_0(cm^{-3})	1.4×10^{15}	4.8×10^{15}
W (μm)	150	170
R_{sh} ($\Omega.cm^2$)	8000	5000
$R_{s,mpp}$ ($\Omega.cm^2$)	0.77	0.35
PFF	82.2	81.5

5. Simulation of the cells

In this section, the Quokka simulation of the best UMG and EGcells are presented. The simulation parameters measured on control wafers for the cells used in the Quokka measured are shown in Table 2.

Table 2. Simulation parameters used in the Quokka simulation of the cells

Side	Properties	Value
Front	Sheet Resistance	120 Ω/□
	ρ_c	0.06 mΩ.cm^2
	$J_{0\text{-}diffused}$	45 fA/cm^2
	$J_{0\text{-}contacted}$	1800 fA/cm^2
	Contact width	10 µm fingers
	Contact spacing	1300 µm
Rear	Sheet Resistance	70 Ω/□
	ρ_c	0.024 mΩ.cm^2
	$J_{0\text{-}undiffused}$	3 fA/cm^2
	$J_{0\text{-}diffused}$	70 fA/cm^2
	$J_{0\text{-}contacted}$	700 fA/cm^2
	Diffusion size	75 µm dot
	Contact size	30 µm dot
	Contact Spacing	300 µm

5.1. Optics

To simulate the J_{sc} accurately in the cells, it is critical to accurately model the wafer optical properties. The optics are modelled using the wafer ray tracer software from PV Lighthouse [28]. The front optics of the cells are modelled with a random textured surface with a Al_2O_3/SiN_x stack with thickness of 15nm/52nm and 15nm/55nm for UMG and EG cells respectively to match our reflectance measurements. This will also account for the slight variation in EQE at wavelengths between 300nm to 500nm. The rear side is modelled with a rear reflector, 0.96 Lambertianfraction, with 95.5%/96% reflectance for UMG/EG cells. The rear reflectance is adjusted until the escape reflectance matches the measured reflectance. Figure 4 shows the measured and simulated reflectance of the cells. The reflectance from the fingers has been subtracted by assuming a constant reflection from the fingers across the whole wavelength range shown in the figure.

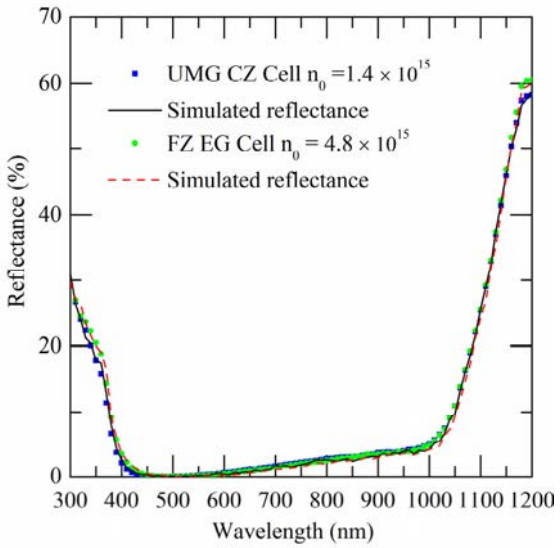

Fig. 4. Measured and simulated reflectance of the cells. The reflectance of the fingers is subtracted from the measurement results.

It is interesting to note that the simulated and measured EQE agrees and UMG and EG cells are almost identical in their EQE in the long wavelength range between 900nm to 1200nm. This indicates that the minority carrier diffusion length is significantly larger than the wafer thickness for both the UMG and EG cells.Although the

minority carrier mobility in the UMG CZ cell is expected to be reduced due to material compensation, the small thickness of the cells and comparable minority carrier lifetimes between UMG and EG cells result in the same EQE in the long wavelength region. The minority carrier diffusion lengths for the UMG and EG cells are estimated to be 695 μm and 1018 μm, with minority carrier mobilities estimated using Schindler's model for UMG [29]and Klaassen's model for EG[30]. The modelled mobilities of both type of wafers are included in Table 3. The compensation in the UMG cell has little effect on the current collection in this case.Thus, the resulting J_{sc} is comparable between the EG and UMG cells shown in Table 4.

5.2. Electric properties

Quokka 3D simulation utilizes the conductive boundary approximation. Thus, the recombination parameters J_0 measured on control wafers for the front and rear surfaces are used to account for the recombination at these boundaries [31]. These parameters are summarized in Table 2. The $J_{0\text{-}contacted}$ for the front and rear are taken from typical values from literatures for a 70Ω/□ phosphorus diffusion [32] and for a 120Ω/□ boron diffusion [33].

As mentioned before, the as-cut bulk lifetime is not representative of the final bulk lifetime. According to the bulk lifetime study in section 3, we are able to use the bulk lifetime post high temperature processing in the simulation. The injection dependent minority carrier lifetime shown in Figure 2 is modelled in Quokka using two defects via the Shockley-Read-Hall (SRH) model to fit the measured lifetime for the EG FZ and UMG CZ samples. Table 3 shows the SRH parameters extracted from the lifetime test structures and used in the simulation of the cells.

Table 3. SRH parameters used in the simulation to reflect the minority carrier lifetime measured in Fig. 2

	E_C-E_T (eV)	σ_n(cm^{-2})	σ_p(cm^{-2})	N_t (cm^{-3})	μ_n ($cm^2V^{-1}s^{-1}$)	μ_p ($cm^2V^{-1}s^{-1}$)
UMG CZ	0.5	1×10^{-18}	5×10^{-17}	1×10^{12}	948.7	372.5
	1	9×10^{-15}	3×10^{-16}	2×10^{12}		
EG FZ	0.5	4×10^{-19}	2×10^{-17}	1×10^{12}	1263	439
	1	2.7×10^{-15}	9×10^{-17}	2×10^{12}		

5.3. Simulation results

Simulation of the *I-V* characteristics of the cells is shown in Figure 3 (a), and is in good agreement with the measured light IV curves for both EG FZ and UMG CZ cells in terms of J_{sc} and V_{oc}. The simulated FF is not in good agreement with the measurements. The simulated FF is much larger than the actual measurements. Quokka simulation only takes the contact resistivity and the bulk electrical properties into account. Any non-ideal processing conditions that may cause resistive losses elsewhere will not be included. The Suns-V_{oc} measurements indicate that series resistance affects the FF in the cells in this case. The PFF is closer to the simulated FF. The device parameters extracted from the simulated light IV are shown in Table 4.

Table 4. Device parameters extracted from the simulated light IV for both UMG CZ and EG FZ cells

Parameters	UMG CZ (simulated)	UMG CZ (measured)	EG FZ (simulated)	EG FZ (measured)
J_{sc} ($mA.cm^{-2}$)	40.36	40.23	40.17	39.89
V_{oc} (mV)	672.75	672.6	687.27	686.2
J_{mpp} ($mA.cm^{-2}$)	38.42	37.03	38.41	37.03
V_{mpp} (mV)	577.11	566.1	597.19	591.7
FF (%)	81.7	77.5 (PFF 82.2)	83.1	80.1 (PFF 81.5)
η (%)	22.22	20.96	22.98	21.91
Δn_{mpp}(cm^{-3})	4.4×10^{14}	-	3×10^{14}	-
Δn_{oc}(cm^{-3})	3.8×10^{15}	-	4×10^{15}	-

The simulation results for both UMG CZ and EG FZ cells are higher than the actual cells. It is almost entirely due to the higher FF from the simulation. The simulated J_{sc} and V_{oc} agree well with the measurements. It indicates the control parameters measured reflects the conditions in the real cells.

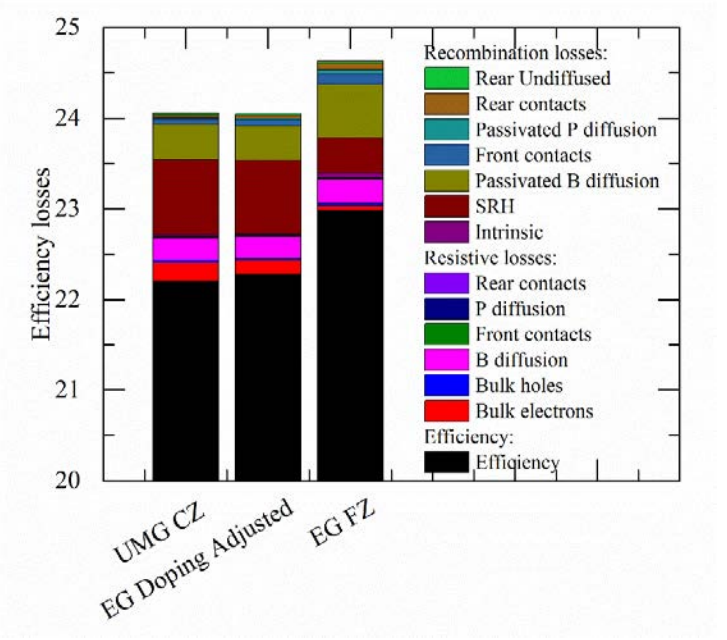

Fig. 5. Power losses using a free energy loss analysis (FELA) in the UMG CZ and EG FZ cells at maximum power point, for ease of reading optics losses are not presented

Figure 5 shows the breakdown of power losses simulated at maximum power point (MPP) using the free energy loss analysis method (FELA) [34]for both UMG CZ and EG FZ cells. FELA is based on the volume integral of photogeneration rate multiplied by the splitting of the quasi-Fermi levels at MPP. The higher efficiency of the EG cell essentially reflects its higher doping, leading to a greater Fermi levels splitting at MPP. A greater Fermi level splitting at MPP (due to doping), also means that losses due to SRH recombination are less significant (they are a smaller fraction of the total power loss) as shown in Figure 5.

Figure 5 also shows that majority electrons resistive losses are greater in the UMG cell compared to the EG cell. However, with these two simulations (with different doping) one cannot clearly conclude if this loss is due to lower doping or lower mobility (or both) of the UMG material. To allow a fair and meaningful comparison between UMG and EG cells we add a third scenario where the net doping of the EG cell is adjusted to the same level as the UMG cell. With this new scenario the UMG cell and EG cell have similar simulated efficiency of 22.2% to 22.28%, respectively. The difference in efficiency is mainly caused by an increased in bulk electron resistive loss in the UMG cell.This reflects the lower mobility in UMG material leading to a lower electron conductivity in the bulk. Contrary to our previous study[20], this effect is apparent dueto the fact that the full-area rear-diffusion is absent in this cell structure and hence cannot assist with majority carrier conduction. All in all however, this effect has a minor influence on the efficiency (0.08% drop).

We note that these devices are also subject to slow degradation under illumination via the boron-oxygen defect, which is described in more detail in [21].

6. Conclusion

In conclusion, we have presented the 3D simulation of silicon solar cells based on 100% UMG CZ wafers with efficiencies of 20.96% and EG FZ cells of 21.91%. From the measurements and simulation, it shows that with an optimised fabrication process, the bulk lifetime and minority carrier diffusion length are not strongly limiting factors for UMG material to achieve high efficiency devices. Excluding resistive losses, the difference in the efficiency between our fabricated EG FZ and UMG CZ cells are mainly due to the difference in net doping.Our simulation shows that at similar doping and with the high quality UMG material used here, the lower majority carrier mobility

is the only factor reducing the efficiency of UMG cells and this effect is minor (<0.1% reduction in efficiency). The simulations also indicate that improved fill factors could lead to efficiencies up to 22% on the UMG substrates with the cell structure developed here.

Acknowledgements

This work has been supported by the Australian Renewable Energy Agency (ARENA) through the Australian Center for Advanced Photovoltaics (ACAP), Project RND009, and their Postdoctoral Fellowships program. DM acknowledges support from the Australian Research Council through the Future Fellowships program.

References

[1] N. Yuge, H. Baba, Y. Sakaguchi, K. Nishikawa, H. Terashima, and F. Aratani, "Purification of metallurgical silicon up to solar grade," *Solar Energy Materials and Solar Cells*, vol. 34, pp. 243-250, 1994.
[2] K.Ounadjela and A. Bloss, New Metallization technique for 6 MW pilot production of multicrystalline solar cells using upgraded metallurgical grade silicon, NREL Technical Report CaliSolar inc. Sunnyvale, 2010.
[3] D. Kohle, B. Raabe, S. Braun, S. Seren, and G. Hahn, "Upgraded Metallurgical Grade Silicon Solar Cells: A Detailed Material Analysis," in *24th European Photovoltaic Solar Energy Conference*, Hamburg, Germany, pp. 1758 - 1761, 2009.
[4] J. Kraiem, B. Drevet, F. Cocco, N. Enjalbert, S. Dubois, D. Camel, *et al.*, "High performance solar cells made from 100% UMG silicon obtained via the PHOTOSIL process," in *Photovoltaic Specialists Conference (PVSC), 2010 35th IEEE*, pp. 001427-001431, 2010.
[5] P. Engelhart, J. Wendt, A. Schulze, C. Klenke, A. Mohr, K. Petter, *et al.*, "R and D pilot line production of multi-crystalline Si solar cells exceeding cell efficiencies of 18%," *Energy Procedia*, vol. 8, pp. 313-317, 2011.
[6] Y. Delannoy, C. Alemany, K.-I. Li, P. Proulx, and C. Trassy, "Plasma-refining process to provide solar-grade silicon," *Solar Energy Materials and Solar Cells*, vol. 72, pp. 69-75, 2002.
[7] K. Hanazawa, N. Yuge, and Y. Kato, "Evaporation of phosphorus in molten silicon by an electron beam irradiation method," *Materials Transactions*, vol. 45, pp. 844-849, 2004.
[8] D. Lynch, "Winning the global race for solar silicon," *The Journal of The Minerals, Metals & Materials Society (TMS)*, vol. 61, pp. 41-48, 2009.
[9] T. Margaria, F. Cocco, J. Kraiem, J. Degoulange, D. Pelletier, D. Sarti, *et al.*, "Status of the Photosil project for the production of solar grade silicon from metallurgical silicon," *Proc. of 25th European PVSC*, pp. 1506-1509, 2010.
[10] I. Santos, A. Goncalves, C. S. Santos, M. Almeida, M. Afonso, and M. J. Cruz, "Purification of metallurgical grade silicon by acid leaching," *Hydrometallurgy*, vol. 23, pp. 237-246, 1990.
[11] S. Pizzini, "Solar grade silicon as a potential candidate material for low-cost terrestrial solar cells," *Solar energy materials*, vol. 6, pp. 253-297, 1982.
[12] Yulia V. Meteleva-Fischer, Yongxiang Yang, Rob Boom, Bert Kraaijveld, and Henk Kuntzel, "Slag treatment followed by acid leaching as a route to solar-grade silicon," *The Journal of The Minerals, Metals & Materials Society (TMS)*, vol. 64, pp. 957-967, 2012.
[13] R. Einhaus, D. Grosset-Bourbange, B. Drevet, D. Camel, D. Pelletier, F. Coco, *et al.*, "Puryfing UMG silicon at the French PHOTOSIL project," in *Photovoltaics International*, pp. 60-65, 2010.
[14] F. A. Trumbore, "Solid solubilities of impurity elements in germanium and silicon*," *Bell System Technical Journal*, vol. 39, pp. 205-233, 1960.
[15] R. Hopkins, R. Seidensticker, J. Davis, P. Rai-Choudhury, P. Blais, and J. McCormick, "Crystal growth considerations in the use of “solar grade” silicon," *Journal of Crystal Growth*, vol. 42, pp. 493-498, 1977.
[16] T. Schutz-Kuchly, J. Veirman, S. Dubois, and D. R. Heslinga, "Light-Induced-Degradation effects in boron–phosphorus compensated n-type Czochralski silicon," *Applied Physics Letters*, vol. 96, 093505, 2010.
[17] F. E. Rougieux, M. Forster, D. Macdonald, A. Cuevas, B. Lim, and J. Schmidt, "Recombination Activity and Impact of the Boron-Oxygen-Related Defect in Compensated N-Type Silicon," *Photovoltaics, IEEE Journal of*, vol. 1, pp. 54-58, 2011.
[18] F. E. Rougieux, B. Lim, J. Schmidt, M. Forster, D. Macdonald, and A. Cuevas, "Influence of net doping, excess carrier density and annealing on the boron oxygen related defect density in compensated n-type silicon," *Journal of Applied Physics*, vol. 110, 063708, 2011.
[19] M. Forster, E. Fourmond, R. Einhaus, H. Lauvray, J. Kraiem, and M. Lemiti, "Ga co-doping in Cz-grown silicon ingots to overcome limitations of B and P compensated silicon feedstock for PV applications," *physica status solidi (c)*, vol. 8, pp. 678-681, 2011.
[20] F. Rougieux, C. Samundsett, K. C. Fong, A. Fell, P. Zheng, D. Macdonald, *et al.*, "High efficiency UMG silicon solar cells: impact of compensation on cell parameters," *Progress in Photovoltaics: Research and Applications*, 2015.
[21] P. Zheng, F. E. Rougieux, C. Samundsett, Xinbo Yang, Yimao Wan, J. Degoulange, *et al.*, "Upgraded Metallurgical-Grade Silicon Solar Cells with Efficiency above 20%," *In Press, accepted for publication in Applied physics letters*, 2016.
[22] A. Fell, "A Free and Fast Three-Dimensional/Two-Dimensional Solar Cell Simulator Featuring Conductive Boundary and Quasi-Neutrality Approximations," *IEEE Transactions on Electron Devices*, vol. 60, pp. 733-738, 2013.

[23] M. A. Green, *Silicon solar cells : advanced principles & practice*. Sydney, Australia: Centre for Photovoltaic Devices and Systems, 1995.
[24] I. Martil and G. G. Diaz, "Determination of the dark and illuminated characteristic parameters of a solar cell from I-V characteristics," *European Journal of Physics*, vol. 13, p. 193, 1992.
[25] D. L. Meier and D. K. Schroder, "Contact resistance: Its measurement and relative importance to power loss in a solar cell," *Electron Devices, IEEE Transactions on*, vol. 31, pp. 647-653, 1984.
[26] R. A. Sinton and A. Cuevas, "A Quasi-Steady-State Open-Circuit Voltage Method for Solar Cell Characterization," in *16th European Photovoltaic Solar Energy Conference*, Hamburg, Germany, pp. 1152–1155, 2000.
[27] D. Pysch, A. Mette, and S. W. Glunz, "A review and comparison of different methods to determine the series resistance of solar cells," *Solar Energy Materials and Solar Cells*, vol. 91, pp. 1698-1706, 2007.
[28] PVLighthouse. (2016). Available: https://www.pvlighthouse.com.au/
[29] F. Schindler, M. C. Schubert, A. Kimmerle, J. Broisch, S. Rein, W. Kwapil, *et al.*, "Modeling majority carrier mobility in compensated crystalline silicon for solar cells," *Solar Energy Materials and Solar Cells*, vol. 106, pp. 31-36, 2012.
[30] D. B. M. Klaassen, "A unified mobility model for device simulation—I. Model equations and concentration dependence," *Solid-State El*ectronics, vol. 35, pp. 953-959, 1992.
[31] A. Fell, "A free and fast three-dimensional/two-dimensional solar cell simulator featuring conductive boundary and quasi-neutrality approximations," Electron Devices, IEEE Transactions on, vol. 60, pp. 733-738, 2013.
[32] A. Cuevas, P. A. Basore, G. Giroult-Matlakowski, and C. Dubois, "Surface recombination velocity of highly doped n-type silicon," Journal of Applied Physics, vol. 80, pp. 3370-3375, 1996.
[33] J. Benick, B. Hoex, M. Van de Sanden, W. Kessels, O. Schultz, and S. W. Glunz, "High efficiency n-type Si solar cells on Al 2 O 3-passivated boron emitters," Appl. Phys. Lett, vol. 92, p. 253504, 253504, 2008.
[34] R. Brendel, S. Dreissigacker, N.-P. Harder, and P. Altermatt, "Theory of analyzing free energy losses in solar cells," Applied Physics Letters, vol. 93, 173503, 2008.